Structural Studies of the Ni-Doped Cu-Cr Ferrites

M. A. Amer and D. El.Kony

Physics Department, Faculty of Science, Tanta University, Tanta, Egypt
drdohaelkony@yahoo.com

Abstract: A series of $Cu1_{-x}Ni_xCrFeO_4$ ferrites, with x = 0, 0.2, 0.4, 0.6, 0.8, and 1, were prepared using the usual ceramic technique. The samples were studied using MÖssbauer,. IR and X-ray patterns. The MÖssbauer spectra were analysed to two magnetic subpatterns A and B and a central paramagnetic phase C. The hyperfine magnetic fields A and B and the paramagnetic phase C are dependent on x, while the isomer shift and quadrupole shift do not show dependence on x. The cation distribution are estimated. Six absorption bands ν_1, ν_2, ν_4, ν_0, ν_A and ν_B were observed in the infrared spectra IR. The Mossbauer parameters and IR peaks revealed the existence of Fe^{2+} ions in the samples. The x-ray patterns confirmed that the samples have a single phase cubic spinel structure of the system. The x-ray parameters show dependence on x-additions.
[M. A. Amer and D. El.Kony **Structural Studies of the Ni-Doped Cu-Cr Ferrites]** Journal of American Science 2012;8(7):836-843]. (ISSN: 1545-1003). http://www.jofamericanscience.org. 122

Key words: Ferrites-MÖssbauer spectra-X-ray-Cation distribution.

1. Introduction

Spinel ferrites are world-wide used in advanced technical designing and applications due to their variety of observed physical properties. Spinel ferrites are magnetic oxides and are one of richest fields refering to large number of compounds. The physical properties of ferrites depend upon the method of preparation, dopant nature and amount of the doping types. Many investigations were carried out on Cu- [1], Ni- [2,3], Cr- [4,5], Cu-Cr- [6-10], Ni-Cr- [11,12], and Ni-Cu- ferrites [13], using Mössbauer, X-ray, infrared patterns and/or other techniques to study their physical and structural properties. The results showed interesting cation distribution, electric and magnetic properties. In our study of the spinel ferrites $CuCr_xFe_{2-x}O_4$ [14], and $Zn_{1-x}Cu_xCr_{0.8}Fe_{1.2}O_4$ [15], we obtaind promised results, which showed signs of relaxation, Jahn-Teller effect and different hyperfine interaction parameters. It is known that in spinel ferrites, Cr^{3+} exclusively occupies the octahedral B-sites and Cu^{2+} and Ni^{2+} preferentially the B-sites [2, 14, 15]. Consequently, this investigation is carried out to study the effect of cation distribution and the interionic distance on the physical and structural properties of the spinel system $Cu_{1-x}Ni_xCrFeO_4$, using Mőssbauer, X-ray and infrared patterns.

2. Experimental

The spinel $Cu_{1-x}Ni_xCrFeO_4$ ferrites, with x = 0, 0.2, 0.4, 0.6, 0.8, and 1, were prepared using the usual ceramic technique mentioned earlier [10,11,14,15]. Proper portions of pure oxide were mixed, ground, heated at 900 ^oC for 20 hrs and cooled down slowly to room temperature. The mixures were ground to fine powder, presed into pellets, sintered at 1200 ^oC for 20 hrs in the normal atmosphere and cooled slowly to room temperature. The X-ray diffraction patterns (will publish elsewhere) revealed that the reflection planes for all samples the existence of a single phase cubic spinel structure of the system.

The Mőssbauer spectra were recorded at room temperature using a 30 m Ci ^{57}Co source in a rhodium matrix, held at room temperature, where metallic iron was used for calibration. The recorded Mőssbauer spectra were analyzed by means of a least-squares fitting computer program, as shown in Fig. 1. The solid lines through the data points are the results of the least squares fit to the experimental data points. The solid lines above the data points are the lines of the individual components. The infrared spectra were recorded in the range from 200 to 4000 cm^{-1}.

3. Results and Discussion

3.1 Spectral analysis

3.1.1 Mőssbauer spectra

Fig. 1 shows the Mőssbauer patterns of the $Cu_{1-x}Ni_xCrFeO_4$ spinel ferrites. They show similar broadened six-line magnetic patterns for all samples and a central paramagnetic phase C for x = 0.0, 0.2 and 1. This broadening may be due to the random distribution of the diamagnetic Cu^{2+} ions among the A- and B-sites, in additi0n to the magnetic Cr^{3+}, Fe^{3+} and/or Ni^{2+} ions. The existence of the phase C may arise from the chemical disorder of the cations at the A- and B-sites or from an isolated number of B-site Fe^{3+} ions within small regions, which can not behave superparamagnetically [16]. The spectra have been analyzed to two magnetic subpatterns A and B. The sharper A attributed to Fe^{3+} ions amongst the tetrahedral A-sites and the broader B attributed to Fe^{3+} and Fe^{2+} amongst the octahedral B-sites. The

broader subpattern B has been fitted with multicomponents B_n, n = 0, 1,.. and 4 (Fig. 1.), n denotes the number of the six A-site Cu^{2+} and/or Ni^{2+} nearest neighbours of the B-site Fe ions. The obtained results from fitting the spectra are listed in Table 1.

Table(1) indicates that the hyperfine magnetic field of the B_n subpatterns decreases with n for all x values, suggesting that the exchange interaction between the magnetic ions at the A- and B-sites is reduced. This reduction increases with n, but the reduction is greater between B_n for $n \geq 1$. The superexchange interaction of each B-cation with its six A-nearest neighbours depends on the distribution of Cu^{2+} and/or Ni^{2+} amongst the six A-cation nearest neighbours, which in turn determines the hyperfine field at the Fe nucleus on the B-sites. The s-electron density at the Fe nucleus is also likely to be dependent on the composition of the six A- nearest neighbours.

Table 1 clears the x dependence of the hyperfine magnetic fields at A-sites H_A and the average at B-sites H_B. It is shown that $H_A > H_B$, and they decrease for $x \leq 0.2$, and increase thereafter. This decrease can be explained on the basis of changing the number of $Fe^{3+}{}_A$ - O^{2-} - $Fe^{3+}{}_B$ bonds and the cation distribution amongst the A- and B-sites [11,14]. The increase of H_A and H_B with $x \geq 0.4$ may be due to the substitution of the magnetic Ni^{2+} for the nonmagnetic Cu^{2+} ions and increasing the number of magnetic ions at both A- and B-sites. Hence the A-B superexchange interaction increases and so do the ferromagnetic interaction between and within the sublattices [11,14].

The isomer shift values δ for the A-sites δ_A are much smaller than those for B-sites δ_B. δ_A is found to lie between 0.02 and 0.24 mm/s and δ_B between 0.08 and 0.48 mm/s. That corresponds to Fe^{3+} in the spinel systems and is characteristics of the high spin Fe^{3+} charge state [15,17]. The high values of δ_B of B_4 for x = 0 and B_0 for x = 0.8 (Table 1), may indicate the existence of Fe^{2+} at these sites. Consequently, the distribution of the s-electron charge of Fe^{3+} ions is influenced by Ni^{2+} substitution. The variations in δ may be result from the change of Fe^{3+} – O^{2-} internuclear separation at A- and B-sites with x.

The relatively high values of quadrupole shift ε_Q (Table 1), indicate the high electric field gradient EFG inside the samples. The A-site ε_{QA} indicate a decreasing trend, while B-sites ε_{QB} indicate an increasing trend with x, in addition to the increase of ε_{QB} with increasing Cu^{2+} and/or Ni^{2+} number as A-site nearest neighbours of B_n at B-site Fe ions. That indicate an increasing deviation from the ideal crystal symmetry (cubic symmetry). The relatively high values of ε_Q of the A- and B-subpatterns, in addition to the higher values of ε_Q of B_4 for x = 0, B_0 for x = 0.8 and B2 for x = 1 (Table 1), indicates the presence of Fe^{2+} ions at the A- and B-sites. That deviation may be due to the Cooperative Jahn-Teller effect of the Fe^{2+}, Cu^{2+} and/or Ni^{2+} at B-sites [15,18]. It may be due to the trigonal distortion of the B-site oxygen coordination i. e. the deformation of the $3d^5$ shell. The change of sign may result frm the chemical disorder, where this disorder can produce a distribution of EFGs of varying magnitude, direction, sign and asymmetry [19].

The outermost line width $\Gamma_{1,6}$ for the B-sites indicates increasing trend against the compositional variation x, while $\Gamma_{1,6}$ for A-sites change randomly. The B/A area ratio increases against x, as indicateded in Table 1, which illustrates that the substitution process increases the number of Ni^{2+} into the A-sites at the expense of Fe^{3+} ions. It is well known that Cr^3 ions exclusively occupy the B-sites and the preferred site for both Ni^{2+} and Cu^{2+} is the B-sites [1-10,14,15]. Hence, the cation distribution of the elements can be deduced as evidenced in Table 2, using the site preference of ions and the concentration ratio of Cu^{2+} and Ni^{2+}number amongst A-site for x = 0 and 1.

3.1.2 Infrared spectra

The recorded IR spectra are illustrated in Fig 2, where six absorption bands ν_1, ν_2, ν_4, ν_0, ν_A and ν_B were observed. The band positions and intensities are given in Table 3. It is clear that the band ν_3 did not appear in the spectra but the shoulder and broadness appeared around ν_2 confirm its presence. The two bands ν_1 and ν_2 are assigned earlier to the complexes of Fe^{3+}-O^{2-} in the A- and B-sites, respectively [10,11,14,15,20-23]. The presence of those two bands in the IR spectra reveals the cubic spinel structure of the system $Cu_{1-x}Ni_xCrFeO_4$. Table 3 clears that the positions and intensities of bands ν_1 and ν_2 are independent on the subtitution factor x. The band ν_4 appeared around 223 cm^{-1} for all x values. It depends on the B-site divalent cations (Cu^{2+}, Ni^{2+} and Fe^{2+}) and is assigned to lattice vibrations of the system [10, 23]. Fig. 4 illustrates other three bands; ν_0 appeared around 890 cm^{-1} only for x =0.6 and 0.8, ν_A lies in the range from 1026 to 1045 cm^{-1} and ν_B in the range from 1112 to 1117 cm^{-1} (Table 3). The bands ν_A and ν_B did not appear in the spectra for $x = 0.2$ and 1, but the shoulder and broadness of the spectra confirm their existence. The band ν_0 is attributed to existence of the Fe^{2+} ions at the A-sites, ν_A is dependent on the Fe^{2+} ions at the A-sites and assigned to the breathing mode of the A-sites or to a compound due to distribution of particle morphologies and ν_B to the highest frequency mode of lattice vibrations [10,22,24,25]. The bands ν_0, ν_A and ν_B were observed in studying some ferrites, using Raman and/or IR spectra [22,24,25], and were assigned to the presence

of the Fe^{2+} in both the A- and B-sites, where increasing the number of Fe^{2+} ions increases their intensities. The bands ν_A and ν_B are affected by the presence of Fe^{2+}-O^{2-} complexes on the A-and B-sites and the distortion of the spinel lattice [10]. Table 3 indicates that the intensity of the bands ν_4, ν_A and ν_B increases with increasing the Ni^{2+} concentration in the samples. This may be explained by increasing the number of the Fe^{2+}-O^{2-} complexes among the A- and B-sites. The Fe^{2+} ions result from the electron hopping between Fe^{3+} and both Ni^{2+} and Cr^{3+} ions. The existence of Fe^{2+} ions in the ferrite sample can cause a shoulder and/or a splitting of the absorption band (Fig. 4). That may reveal the existence of local deformations due to Jahn-Teller effect in Fe^{2+}, Ni^{2+} and Cu^{2+} ions [10, 24].

3.1.3 X-ray data analysis

Fig. 3 shows the X-ray diffraction patterns of the prepared ferrite sampels $Cu_{1-x}Ni_xCr\ Fe\ O_2$.The reflection from the planes (111), (220), (311), (222), (440), (422), (511), (440), (620), (533), (622) and(444) appeared for all samples.This reveals that these samples are spinel ferrites and have one single cubic phase.The diduced values of the lattice parameter α for all samples from the X-ray patterns was calculated using the equation ,

$$a^2 = \frac{\lambda^2(h^2 + K^2 + L^2)^{1/2}}{4sin^2\theta}$$

Where λ is the wave length of X-ray radiation ,θ is the Bragg angle and hkl are the indices of the Plane.The value of the lattice parameter α is found to be lie between 8.3412 and 8.353A°

Fig.(4a) illustrate the calculated values of lattice constant α as function of the Ni content x, the lattice constant is found to decrease with increasing x up to x=0.8 then increase slightly.

The particle size was estimated from the reflected lines of the X-ray diffraction pattern of the composites using the Sherrer equation

$$D = \frac{k\lambda}{h_{1/2}cos\theta}$$

Where the constant k=0.9 and $h_{1/2}$ is the half width of the reflected peak of the (hkl) plane.

The X-ray density (theoretical density) was calculated using the formula Dx=8M/_N α3_kg m-3

where 8 represents the number of moleculs in the unit cellof spinel lattice ,M represents the molecular weight of the sample,N is Avogadro's number and α is the lattice parameter.

Fig(4b) shows that theX-ray density ,D_x, decrease with increasing x (Ni content) since the atomic weight of Ni ion(=58.71) is less than that of Cu ion (=63.54).

The cation distribution for spinel ferrites having the formula $Me\ Fe_2O_4$ can be expressed as

$Me_\delta\ Fe_{1-\delta}\ [\ 'Me_{1-\delta}\ Fe_{1+\delta}\ ]O_4$ where δ is the fraction which can determine the cation distribution.

For the composition $Cu_x\ Ni_{1-x}\ Cr\ Fe\ O_4$ the cation distribution can be expressed as:

$Ni_\delta\ Cu_\gamma\ Fe_{(0.5-\gamma-\delta)}\ [\ Ni_{(x-\delta)}\ Cu_{(1-x-\gamma)}\ Cr\ Fe_{(0.5+\gamma+\delta)}\ ]$

In this case the mean ionic radius of the A-and B-sublattices (R and R)can be calculated for all samples using the cation distributions shown in table(2) and the relations:

$R_A = \delta\ r_{Ni} + \gamma\ r_{Cu} + (0.5-\delta-\gamma)\ r_{Fe}$

$R_B = 1/2[\ (x-\delta)\ r_{Ni} + (1-x-\gamma)\ r_{Cu} + r_{Cr} + (0.5+\delta+-\gamma)\ r_{Fe}]$

Where r denotes to the ionic radius and δ,γ denotes to the number of the Ni^{2+} or Cu^{2+} ions at the A-sites ,the calculated values are plotted versus x- in fig. (4c).

The oxygen parameter (u) can be determined using the relation :

$R_A = \alpha\ 3\ (u - 0.25) - r_0$

or

$R_B = \alpha\ (\ 5/8 - u\ ) - r_0$

Where r is the radius of the oxygen ion. The oxygen parameter is a quantitative measure of the displacement of oxygen ions surrounding a tetrahedral site which are too small to contain metal ions

The tetrahedral bond length d_{AO} (d_{A-O}) and the octahedral bond length d_{BO}(d_{B-O}) can be obtaind using the relations :

$d_{AO} = \alpha\ 3\ (\ u - 0.25\ )$

$d_{BO} = \alpha\ (3\ u^2 - 11/4\ u + 43/64\ )^{1/2}$

The tetrahedral edge dAE, octahedral edge d_{BE} and unshared edge d_{BEU} can be calculated using the relations :

$d_{AE} = \alpha\ 2\ (2u - 0.5)$

$d_{BE} = \alpha\ 2\ (1 - 2u\ )$

$d_{BEU} = \alpha\ (\ 4\ u^2 - 3u + 11/16\ )^{1/2}$

The obtaind values of all these parameters are given in Table (1)

Corresponding author
D. El. Kony
Physics Department, Faculty of Science, Tanta University, Tanta, Egypt
drdohaelkony@yahoo.com

Table 1. Mössbauer parameters of the $Cu_{1-x}Ni_xCrFeO_4$ ferrites, H, δ, ε_Q (ΔE), $\Gamma_{1,6}$ and A_0 are the hyperfine magnetic field, the isomer shift, the quadrupole shift (or the quadrupole doublet splitting), the outermost linewidth and the fractional area of the corresponding subpattern, respectively.

X	subpattern	H(T)	δ (mm/s)	ε_Q (mm/s)	$\Gamma_{1,6}$(mm/s)	A_0
0	A	36.45	0.02	-0.04	1.56	0.51
	B_0	41.58	0.23	0.13	0.51	0.07
	B_1	39.1	0.26	0.07	0.75	0.11
	B_2	35.88	0.41	0.17	0.88	0.13
	B_3	29.59	0.3	- 0.05	1.07	0.08
	B_4	22.58	0.48	0.51	0.85	0.05
	C	-----	0.18	0.57	0.37	0.07
0.2	A	34.77	0.14	0.17	1.45	0.47
	B_0	39.97	0.17	0.24	0.43	0.04
	B_1	37.41	0.32	- 0.15	0.94	0.08
	B_2	30.71	0.27	- 0.24	1.56	0.16
	B_3	28.49	0.14	0.27	1.03	0.11
	B_4	20.88	0.26	0.28	1.45	0.1
	C	------	0.17	0.55	0.35	0.04
0.4	A	34.84	0.07	0.01	1.49	0.44
	B_0	39.01	0.44	0.06	0.61	0.06
	B_1	38.7	0.13	0.03	0.61	0.1
	B_2	34.5	0.44	0.15	1.1	0.13
	B_3	27.71	0.22	0.24	1.51	0.2
	B_4	16.71	0.4	0.28	1.12	0.07
0.6	A	35.79	0.05	0.02	1.65	0.42
	B_0	41.12	0.22	0.02	0.41	0.04
	B_1	38.09	0.18	- 0.02	0.72	0.12
	B_2	36.57	0.5	0.25	1.34	0.19
	B_3	28.97	0.25	0.04	1.28	0.12
	B_4	18.94	0.23	0.12	1.69	0.11
0.8	A	38.89	0.05	-0.03	1.12	0.41
	B_0	50.93	0.62	- 0..93	0.56	0. 03
	B_1	47.13	0.1	-0.1	0.96	0. 09
	B_2	39	0.47	0.15	0.85	0.17
	B_3	31.42	0.08	0.02	1.12	0.18
	B_4	17.51	0.29	0.34	2.15	0.12
1	A	47.7	0.24	-0.03	1.53	0.4
	B_0	48.92	0.39	-0.18	0.58	0.08
	B_1	48.47	0.22	- 0.31	0.76	0.12
	B_2	27.16	0.41	0.38	1.62	0.22
	B_3	18.8	0.25	-0.02	0.96	0.11
	C	----	0.28	0.41	0.84	0.07
Error		± 0.05	± 0.01	± 0.02	± 0.01	± 0.01

Table 2. Cation distribution of the spinel system $Cu_{1-x}Ni_xCrFeO_4$.

x	A-sites	B-sites
0	$Cu_{0.49}Fe_{0.51}$	$Cu_{0.51}Cr_1Fe_{0.49}$
0.2	$Ni_{0.13}Cu_{0.4}$ $Fe_{0.47}$	$Ni_{0.07}Cu_{0.4}Cr_1Fe_{0.53}$
0.4	$Ni_{0.26}Cu_{0.3}Fe_{0.44}$	$Ni_{0.14}Cu_{0.3}Cr_1Fe_{0.56}$
0.6	$Ni_{0.38}Cu_{0.2}Fe_{0.42}$	$Ni_{0.22}Cu_{0.2}Cr_1Fe_{0.58}$
0.8	$Ni_{0.48}Cu_{0.11}Fe_{0.41}$	$Ni_{0.32}Cu_{0.09}Cr_1Fe_{0.59}$
1	$Ni_{0.6}$ $Fe_{0.4}$	$Ni_{04}Cr_1Fe_{0.6}$

Table 3. The infrared absorption bands ν_n and their intensities I_n, where n = 1, 2, 4, A and B for the $Cu_{1-x}Ni_xCrFeO_4$ ferrites.

x	ν_1 (cm^{-1})	I_1	ν_2 (cm^{-1})	I_2	ν_4 (cm^{-1})	I_4	ν_A (cm^{-1})	I_A	ν_B (cm^{-1})	I_B
0.0	588	3.5	504	4.9	223	3	1045	45	1117	39.7
0.2	586	3.2	492	4.4	223	7.9	----	----	----	----
0.4	599	3.4	495	7.5	223	10.9	1026	55.8	1115	59.8
0.6	602	6.9	506	8.7	223	12.8	1044	53	1125	32.1
0.8	594	3.8	498	6.8	223	14.5	1041	61	1112	74.3
1	592	3.3	490	4.9	223	16.6	-----	-----	-----	-----
Error	± 1	± 0.2	± 1	± 0.2	± 1	± 0.2	± 1	± 0.2	± 1	± 0.2

Tble 4. The bond length of the A-sites d_{AL} and B-sites d_{BL}, the tetrahedral edge d_{AE}, the octahedral shared edge d_{BE} and unshared edge d_{BEU} and the hopping length at the A-sites L_A and B-sites L_B for the system $Cu_{1-x}Ni_xCrFeO_4$.

x	d_{AL}(Å)	d_{BL} (Å)	d_{AE} (Å)	d_{BE} (Å)	d_{BEU}(Å)	L_A (Å)	L_B (Å)
0.0	2.018	1.975	3.2946	2.6118	2.9631	3.61696	2.9532
0.2	2.001	1.9823	3.2675	2.6369	2.9605	3.6156	2.9521
0.4	2.0019	1.9787	3.26904	2.6294	2.9579	3.6121	2.9492
0.6	2.299	1.913	3.7415	2.1502	3.006	3.6157	2.9522
0.8	2.0051	1.977	3.2744	2.6237	2.95799	3.6118	2.9491
1	2.0099	1.9774	3.2822	2.6215	2.9611	3.6153	2.9519

Error = ± 0.0001

Table 5. The X-ray density, Saturation Magnetization , crystallite size ,lattice parameter ,and magnetic susceptibility for the system Cu1-xNixCrFeO4.

X	D_x gm/cm^3	M_s emu/g	D	α A^0	$\chi*10^{-6}$ c.g.s
0.0	5.3648	17.82	11.3704	8.353	16900
0.2	5.3488	18.36	11.372	8.3499	10900
0.4	5.3425	16.2	9.4816	8.34169	11800
0.8	5.2993	14.04	11.3778	8.34116	16500
1	5.2614	6.48	9.4778	8.34912	34000

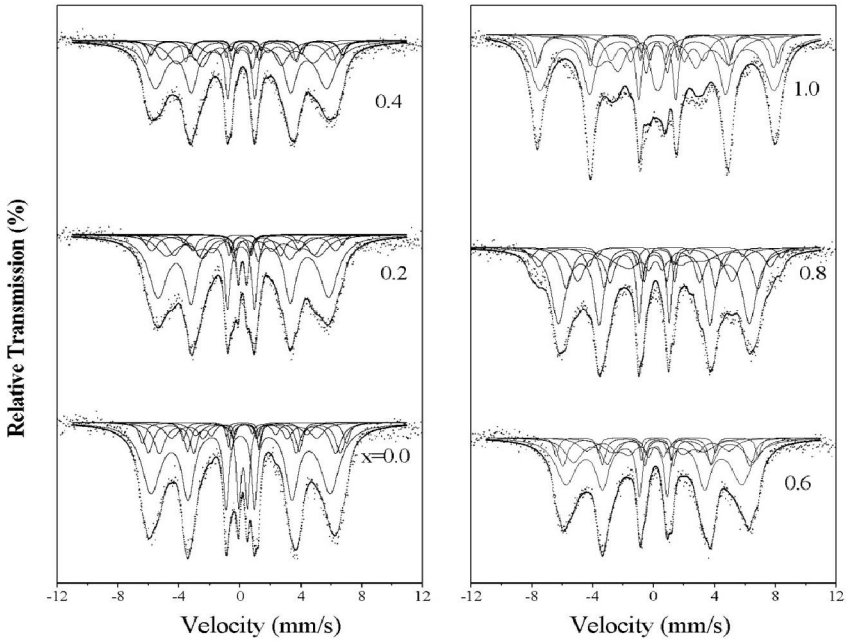

Fig 1. The Mőssbauer patterns of the $Cu_{1-x}Ni_xCrFeO_4$ spinel ferrites

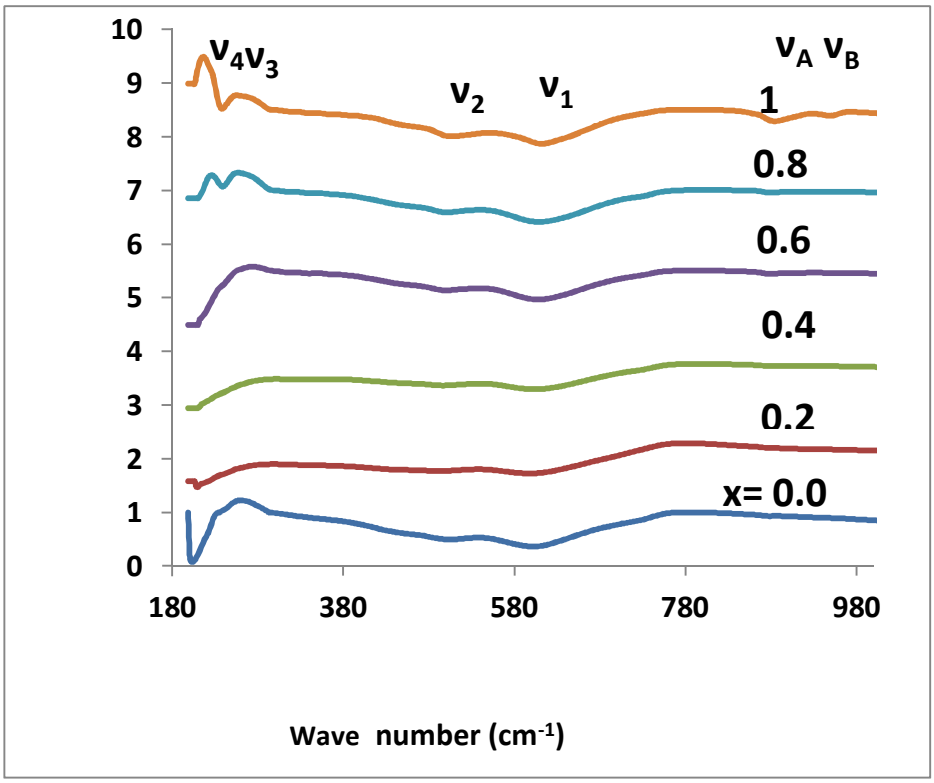

Fig (2) Wave number

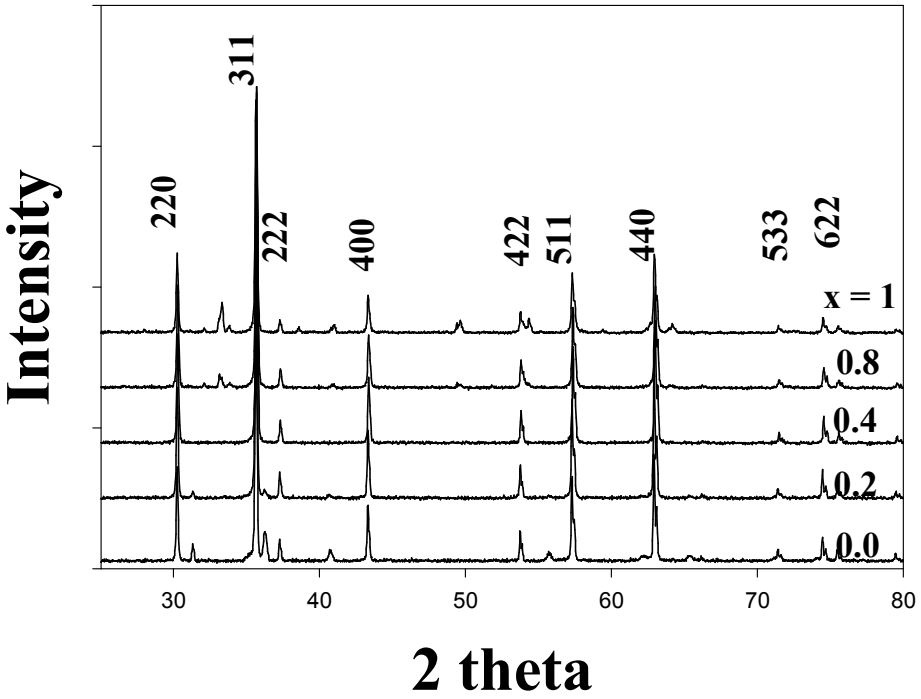

Fig (3) The X-ray patterns of the $Cu_{1-x}Ni_xCrFeO_4$ spinel ferrites

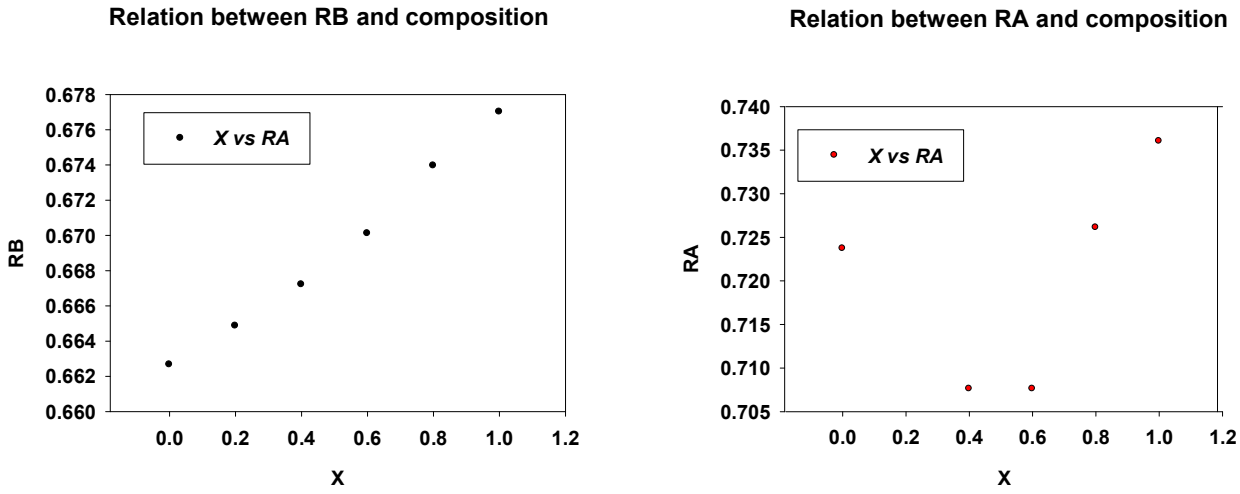

Fig.(4c)

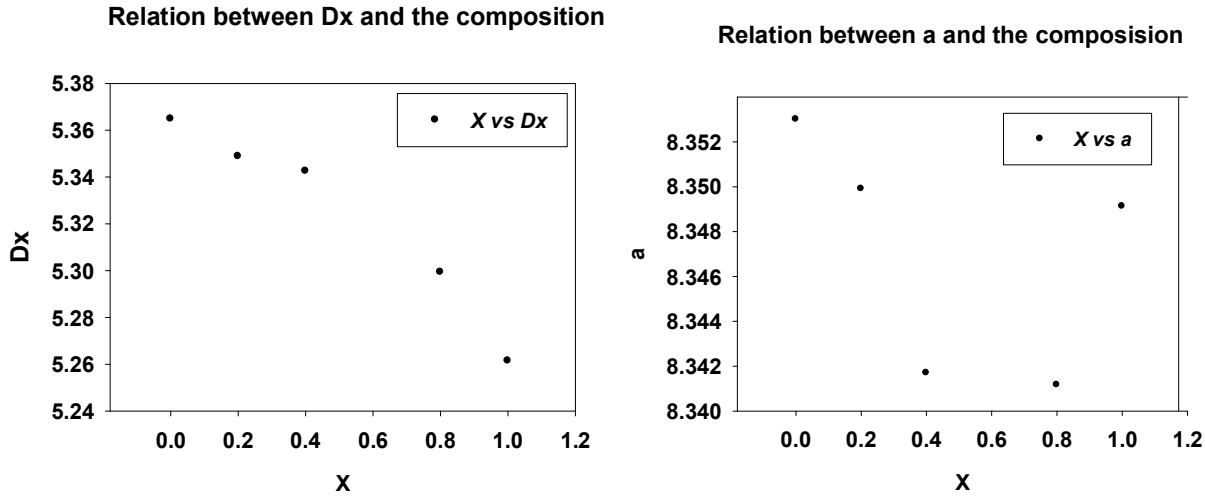

Fig.(4a,b)
Fig (4) Relatinship

References

1- Rana M. U. and Abbas T.,(2002), J. Mag. Mag. Mater. 246/1. 110.
2- Amer M. A. and El Hiti M.A.(2001) ,J. Mag. Mag. Mater. 234:118.
3- Corso S.,Tailhades P.,Rasquet I., Rousset A.,. V. Laurent, Gabriel A. and Condolf C., (2004), Sol. State Sci. 6/8 791.
4- Chae K. P., . Lee Y. B., . Lee J. G and. Lee S. H., (2000) J. Mag. Mag. Mater. 220/1 :59.
5- Lee S. W., . An S. Y., Kim S. J. and. Kim C. S., (2002) J. Mag. Mag. Mater. 239/1 :76.
6- An D. H.,Kang K. U.,Lee B. G,Lim J. B.,Jang S. U.,Baek K. S. and Ok H. N., (2003)
Phys. J. Phys. Chem. Solids 64/12:2351.
7- Yunus S. M., . Shim H. S, Lee C. H., . Asgar M. A, Ahmed F. U. andA. Zakaria K. M., (2002). J. Mag. Mag. Mater. 2 41/1:40.
8- Singh G. and Darshane V. S., (1994), J. Mater. Sci. 29, 1540.
9- Okasha N., (2004) Mater. Chem. And Phys. 84/1:63.
10- Amer M. A., (2003) Phys. Stat.Sol. (b) 237, No . 2, 459.
.11- Amer M,. Ata-Allah S., Meaz T., Aboul- Enein S. and. Abd-Elhamid M., (2005). Turk. J. Phys. 29:163.
12- Zakaria A. K. M., . Asgar M. A, Eriksson S. G., Ahmed F. U., Yunus S. M., Azad A.K. and Rundlif H., (2003) Mater. Letters 57/26-27 : 4243.

13- Kim W. C., Kim S. J. and Kim C. S., (2002) J. Mag. Mag. Mater. 239/1:82.
14- Amer M. A., Ahmed M. A., Elnimr M. K. and Mustafa M. A., (1995) Hyperfine Interact. 96:91.
15- Amer M. A., (2000) Phys. Stat. Sol. (a) 181:539.
16- Grave E. De, Covaert A., Chambaere D. and Robbrecht C., (1979) J. Phys. Collog. 40/C2,:669.
17- Ok H. N., Baek K. S., Lee H. S. and Kim C. S., (1990). Phys. Rev. B 41:62.
18- Sturge M. D., (1965) , Phys. Rev. 140, A880.
19- Ok H. N.and Evans B. J., (1976) , Phys. Rev. B, 14:, 2956.
20- Mahmoud M. H., Abd-Elrahman M. I., Abdalla A. M. and Abdel-Mageed A. I., Phys. Stat. Sol. (b) 226/2 (2001) :369.
21- Shaikh A. M., Watawe S. C., Jadhav S. A. and chougule B. K., Mater. Researh Bullet. 37/15 (2002) :2547.
22- Baraton M. I., Lorenzelli V. , Busca G. and WIilley R. J., J. Mater. Sci. Letters 13 (1994) :275.
23- Watawe S. C., Sutar B. D., Sarwade B. D. and Chougule B. K., Internat. J. Inorg. Mater., V3/7 (2001) :819.
24- Potokova V. A., Zverv N. D. and Romanov V. P., Phys. Stat. Sol. (a) 12 (1972) :623.
25- El-Nimr M. K., Ahmed M. A. and El-Hiti M. A., J. Mater. Sci. Letters 13 (1994) :1500.
26- Hemeda O. M., J. Mag. Mag. Mater. 36-41 (2004) :281.
27- Neumann J., Rawe M., Veenhuis H., Pankrath R., Krayzig E., Phys. Stat. Sol. (B) 215 (1999) : R9.
28- Hughes A. E. and Pooley D. "Real Solids and Radiations" Vol. 39, WYKham Publ. Limited, London, 1975.
29- Hemeda O. M. and Barakat M. M. , J. Mag. Mag. Mater. 323 (2001) :127.
30- C. Prakash and J. S. Baijal, J.Less-Common Method 106 (1985) :257.
31- P. K. Roy and J. Bera, J. Mag. Mag. Mat. 298 (2006) :38.

6/9/2012